RSC Advances

# Aquatic biomass containing porous silica as an anode for lithium ion batteries



| | |
|---|---|
| Journal: | *RSC Advances* |
| Manuscript ID: | RA-COM-06-2014-006420.R2 |
| Article Type: | Communication |
| Date Submitted by the Author: | 13-Aug-2014 |
| Complete List of Authors: | Lisowska-Oleksiak, Anna; Gdansk University of Technology,<br>Nowak, Andrzej; Gdansk University of Technology,<br>Wicikowska, Beata; Gdansk University of Technology, |
| | |

# Aquatic biomass containing porous silica as an anode for lithium ion batteries

**Anna Lisowska-Oleksiak*, Andrzej P. Nowak, Beata Wicikowska**

Faculty of Chemistry, Department of Chemistry and Technology of Functional Materials
Gdańsk University of Technology, Narutowicza 11/12, 80-233 Gdańsk, Poland
*email: alo@pg.gda.pl

## Abstract

A composite electrode was manufactured by pyrolysis of Red Algae (*Polysiphonia fucoides)* covered by diatoms (*Diatomophyceae*). Electrodes were tested as a half cell with capacity of 500 mAh/g after 80 cycles. XPS analysis shows formation of lithium silicate under reduction of silica in an aprotic electrolyte containing $LiPF_6$ salt.

*Keywords*: Diatoms, anode, silica, lithium ion batteries.

## 1. Introduction

Electroactivity of silica has attracted attention as a potential anode for lithium ion batteries (LIBs) [1–5]. The four electron reduction of $SiO_2$ may lead to formation of silicate and silicon. The other reduction path is irreversible with silicon and lithium oxide as the products [3]. Electroactivity of $SiO_2$ had been found to be related to the grain size of oxides. There are several examples of successful performance of nanostructured silica used as anodes in LIBs, among them laboriously created hollow porous nanocubes were proposed [6]. Beach sand was also tested and high energy mechanical milling was carried out to reach the appropriate grain size reduction of the oxide to be active under lithiation [7]. Another source of very fine silica is on hand. It is commonly known that naturally occurring amorphous silica of high porosity is available from aquatic biomass containing diatoms [8].

In this work we focus on electrochemical activity of electrode materials produced from pyrolysed sea water biomass. Considering the structure and surface modification of silica, we chose naturally occurring matter in the form of Red Algae *Polysiphonia fucoides,* covered by diatoms (*Diatomophyceae*). The diatoms part acts as a highly porous silica source while Red

Algae deliver the carbonaceous part of the composite. XPS analysis has been employed for identification of electrode reaction products.

## 2. Experimental

The material was prepared from sea water biomass, namely red algae *(Polysiphonia fucoides)* covered by diatoms from the Baltic Sea, by thermal treatment according to the procedure given in Patent Application [9]. The electrodes (referred to as RAD) were prepared from a slurry (90 wt.% of active material, and 10 wt.% of binder (polyvinylidene fluoride PVdF, Sole, Germany) in NMP on ~10 μm thin copper foil (Schlenk Metallfolien GmbH & Co KG, Germany). Dried disc electrodes were used in two-electrode Swagelok® cells with lithium foil as the counter and reference electrodes.

Cyclic voltammetry (cv) was performed using an electrochemical potentiostat/galvanostat Autolab (PGStat302N, The Netherlands) between 0.01 (±0.004) – 3.2 (±0.004) V versus $Li/Li^+$ at a scan rate of 100 $\mu V \cdot s^{-1}$. All measurements were performed at 21 (±1) $^oC$. For battery tests the electrochemical measurements were performed in two electrode Swagelok® type cells with active material as the working electrode and lithium foil (99.9% purity, 0.75 mm thickness, AlfaAesar, Germany) as the counter/reference electrode. In the case of pure aerogel the electrode was prepared from a slurry: 50 wt.% of $SiO_{2ag}$, 30 wt.% of carbon black (Super P, Timcal, Switzerland) and 20 wt.% of binder (polyvinylidene fluoride PVdF, Sole, Germany) in NMP. In all cases the assumed capacity of the composite material was taken as 372 mAh/g for comparison to the graphite electrode. A battery charging at a rate of C/20 (C-rate) will deliver its nominal evaluated capacity in 20 h.

Micro-Raman spectra were recorded on a Raman spectrometer inVia Renishaw (Renishaw, England) with an Ar ion laser at a wavelength of 514 nm. The spectral analysis was performed with GRAMS/32 (Galactic) software with the Lorentzian fitting procedure with 5 peaks ($\chi^2$= 1.31±0.2).

X-ray Photoelectron Spectroscopy (XPS) measurements (Thermo Fisher Scientific) were carried out at base pressure of ~$1 \cdot 10^{-9}$ mbar with Al Kα monochromatized radiation (hν = 1486.6 eV) as the X-ray source. The binding energies were corrected by setting the C 1s hydrocarbon peak at 285.0 eV.

**3. Results and discussion**

The chemical composition of composite was determined by Energy Dispersive X-ray (EDX) analysis. The composite consists of carbon (~ 38 at. %), Si (12 at. %), oxygen (43 at. %) and other elements: Na, Mg, Al, P, S, K, Ca, Fe in small amounts of 1.30, 0.11, 0.62, 0.04, 0.005, 0.006 ± 0.1% [norm at.%], respectively. The presence of these elements is typical for macroalgae biomass [8].

The Scanning Electron Microscopy (SEM) image of pyrolysed biomass before milling has been shown in Fig. 1. Red algae and diatoms preserved their skeleton morphology despite pyrolysis. Fibrous, long elements (from red algae) are covered with polyhedron skeletons. The diatoms are located randomly. The average size of the shells is ~ 30 μm. The porosity of diatoms is illustrated in the inset, where regular, square voids (of ~ 100 nm side) have been shown.

The Raman spectrum of pyrolysed biomass has been presented in Fig. 2. The band at 430 $cm^{-1}$ has been ascribed to the Si-O bond in $SiO_2$ [10]. The presence of maxima at ~ 1350 $cm^{-1}$ and 1585 $cm^{-1}$ are typical for disordered carbonaceous material [11]. The analysis of Raman spectrum in the range 1000 – 2000 $cm^{-1}$ should be performed with 5 bands [12]. The meaning of bands D and G is similar to that given in Ref. [13]. The meaning of three additional bands is as follows: D2 and D4 are attributed to the disordered graphitic lattice while the D3 band originates from the amorphous carbon phase [14,15]. The ratio of intensities *I(D)* to *I(G)* gives possibility for coarse estimation of the cluster size, $L_a$ [11]. The $L_a$ parameter is equal to 24 Å.

The broad maximum in the range 2500 – 3000 $cm^{-1}$ historically has been named G′ and it is very often present in graphitic materials [16]. The G′ band has nothing to do with the G peak, but is the second order of zone-boundary phonons corresponding to the overtones and combinations of graphitic lattice vibration modes [17]. Thus, the presence of a peak at ~ 2800 $cm^{-1}$ confirms the presence of $sp^3$ (diamond-like) bonds from $C/H_x$ stretching modes [13].

The material characterised above was used for electrode preparation, see Experimental.

The first two cyclic voltammetry (cv) curves of studied material are shown in Fig. 3. The cathodic current growth, recorded at the threshold potential $E_{th}$= 0.98 V, is much higher at the first scan due to solid electrolyte interphase formation (SEI) [6]. This process appears at the same potential range, where electrode material undergoes reduction. On the reverse scan the products of reduction are oxidized and both cv curves are similar in shape.

The material was tested using galvanostatic cyclic polarization. The data for the $20^{th}$ and the $80^{th}$ charging/discharging cycles with change of the capacity, depending on the applied current and number of cycles, have been shown in Fig. 4. The electrode exhibits a capacity drop between the first and the second scan, see inset in Fig. 4, as expected for solid electrolyte interphase (SEI) formation [6]. The charge capacity for rates C/20 is equal to 530 mAh/g with capacity retention of 88% over 5 cycles. After increasing the current (C/10 – rate) the capacity diminishes to 467 mAh/g with capacity retention of 97% for the $5^{th}$ cycle. At the C/5 – rate the capacity is equal to 419 mAh/g without significant fading (~ 1 %) over 5 cycles. When a low current was applied again (C/20 – rate, 18 mA/g), the capacity of ~ 500 mAh/g was achieved over 80 cycles a with capacity retention of 94%. This result is close to data presented by other authors for silica nanoparticles coated by carbon [4]. The authors reported a capacity of 500 mAh/g for current density equal to 50 mA/g after the $50^{th}$ cycle. The best

results of capacity ~ 1000 mAh/g for current density of 100 mA/g were achieved for laboriously tailored hollow porous silica nanocubes [6] and high energy milled quartz [7].

The cycling properties at higher rates have been shown in Fig. 5. The first five cycles were performed to activate electrode material including SEI formation. Thus, these cycles were not shown in Fig. 5. The following 20 cycles for each C – rate- exhibit capacities of 362 mAh/g for 1C, 274 mAh/g for 2C, 212 mAh/g for 5C and 141 mAh/g for 10C. The capacity retention after 20 cycles was 99.17 %, 98.20 %, 98.60 % and 98.53 % for 1C, 2C, 5C and 10C, respectively.

The RAD electrode shows quite stable cyclic performance with relatively high capacities for slow C- rates. The higher currents give non-rewarding capacities and limit the usage of such electrodes for high power application. However, it was shown that the presence of carbon particles is very likely to influence the current rate and capacity values. Thus, better electrochemical performance is expected to be achieved by optimization of the carbon amount in the sample and interaction between silica particles and the electronic conductor.

In order to identify products of electrode reactions, XPS analysis was performed for the pristine electrode, for the reduced (charged) electrode and the oxidized (discharged) electrode.

The C 1s spectrum for all studied materials, shown in Fig. 6a, exhibits several peaks in the range 283 – 291 eV, attributed to C-C, C-H and $CO_x$ groups [18–25].

For the O 1s spectrum (Fig. 6b) peaks between 528 – 533 eV are ascribed to Me-O, Si-O, $CO_x$ groups as is given in Refs. [18,23,26–28].

In Si 2p the signals in the range 101 – 103 eV are recorded for all samples, see Fig. 6c. The signals between 100.60 – 102.40 eV can be attributed to the Si-Li bond in $Li_xSi$ [3], as well as the Si-O bond in $SiO_x$ and/or $Li_xSiO_y$ [19,20]. Presence of signals at ~ 102.60 – 103.60 eV is attributed to the Si-O bond in $SiO_2$ [20,29,30].

Thus, since the pristine material mainly contains $SiO_2$ and some amount of metal oxides, it has been proved that $Li_xSiO_y$ and $Li_xSi$ are present in the charged material. However, not all $SiO_2$ reacts with $Li^+$ during cathodic polarization. After the discharging process, the material consisted of $SiO_2$ and MeO, as observed for pure material.

Taking into account the results from galvanostatic cyclic polarization and XPS we confirmed lithium silicates formation according to reactions given in Ref. [6]:

$$5\ SiO_2 + 4\ Li^+ + 4\ e^- = 2\ Li_2Si_2O_5 + Si \quad (1)$$

$$2\ SiO_2 + 4\ Li^+ + 4\ e^- \rightarrow Li_4SiO_4 + Si \quad (2)$$

The obtained Si reacted further with lithium ions with lithium silicide formation:

$$5\ Si + 22\ Li^+ + 22\ e^- = Li_{22}Si_5 \quad (3)$$

No lithium oxide was identified by XPS analysis, being advantageous as electroreduction of silica leading to the $Li_2O$ product is irreversible as reaction (2) opposite to reaction (1) [6].

**4. Conclusions**

Aquatic biomass in the form of red algae covered by diatoms has been found to be a source of electronic conductor (carbon) and substrate for faradaic reactions (silica) if treated thermally and mechanically.

The electrode material obtained from pyrolysed material has been characterized by SEM, Raman spectroscopy and electrochemical techniques. The material mainly consists of silica and the carbonaceous part. The XPS measurements confirm formation of $Li_xSiO_y$ and $Li_xSi$ during electroreduction of silica in contact with $LiPF_6$ in EC/DMC electrolyte.

The galvanostatic charging/discharging test gives a capacity of 419 mAh/g for the C/5 – rate. Slow cycling (C/20 –rate) allows a higher capacity above 500 mAh/g over 80 charging/discharging cycles to be achieved. For higher current rates the capacity is lower due to faradaic current kinetic limitations. It is worthy to work on the size of the particles as it was

performed for pure silica [31] or to take into account the incorporation into carbon nanotubes as it was done for some alloy system [32].

Aquatic biomass was successfully used for anode preparation for Li – ion batteries. Activity of the electrodes relies on the porous silica part resulting from diatoms. The porous structure of diatoms, being a naturally formed nanostructure, preserves the proper condition for good electrode performance. The application of naturally occurring nano-materials saves energy during technological steps and is in general less expensive than manufacture from scratch.

Here we have shown that nanoporous silica is readily available in the form of diatoms and can by used as an active electrode material achieving promising capacity for application in lithium ion batteries.

**Acknowledgments**

We gratefully acknowledge the financial support from the National Science Centre, Kraków, Poland (NN 1503/B/H03/2011/40).

**Reference**

[1] J. Yang, Y. Takeda, N. Imanishi, C. Capiglia, J.Y. Xie, O. Yamamoto, Solid State Ionics 152-153 (2002) 125.

[2] Q. Sun, B. Zhang, Z.-W. Fu, Appl. Surf. Sci. 254 (2008) 3774.

[3] B. Guo, J. Shu, Z. Wang, H. Yang, L. Shi, Y. Liu, L. Chen, Electrochem. Commun. 10 (2008) 1876.

[4] Y. Yao, J. Zhang, L. Xue, T. Huang, A. Yu, J. Power Sources 196 (2011) 10240.

[5] C.-H. Doh, H.-M. Shin, D.-H. Kim, Y.-C. Ha, B.-S. Jin, H.-S. Kim, S.-I. Moon, A. Veluchamy, Electrochem. Commun. 10 (2008) 233.

[6] N. Yan, F. Wang, H. Zhong, Y. Li, Y. Wang, L. Hu, Q. Chen, Sci. Rep. 3 (2013) 1568.

[7] W.-S. Chang, C.-M. Park, J.-H. Kim, Y.-U. Kim, G. Jeong, H.-J. Sohn, Energy Environ. Sci. 5 (2012) 6895.

[8] D. Werner, The Biology Of Diatoms, University of California Press, 1977.

[9] A. Lisowska-Oleksiak, A.P. Nowak, B. Wicikowska, Sposób Otrzymania Anod Ogniw Litowo-Jonowych Poprzez Użycie Ziemi Okrzemkowej I/lub Okrzemek, 2014.

[10] C. Washington, Phys. Rev. Lett. 57 (2000) 2.

[11] F. Tuinstra, J.I. Koenig, J. Chem. Phys. 53 (1970) 1126.

[12] A. Sadezky, H. Muckenhuber, H. Grothe, R. Niessner, U. Pöschl, Carbon N. Y. 43 (2005) 1731.

[13] A.C. Ferrari, J. Robertson, Phys. Rev. B 61 (2000) 14095.

[14] Y. Wang, D.C. Alsmeyer, R.L. Mccreery, Chem. Mater. 2 (1990) 557.

[15] B. Dippel, H. Jander, J. Heintzenberg, Phys. Chem. Chem. Phys. 1 (1999) 4707.

[16] M. Pimenta, G. Dresselhaus, M.S. Dresselhaus, L.G. Cançado, A. Jorio, R. Saito, Phys. Chem. Chem. Phys. 9 (2007) 1276.

[17] P. Dhamelincourt, J. Laureyns, Carbon 32 (1994) 1523.

[18] H. Nara, T. Yokoshima, M. Otaki, T. Momma, T. Osaka, Electrochim. Acta 110 (2013) 403.

[19] B. Philippe, J. Allouche, F. Lindgren, M. Gorgoi, D. Gonbeau, K. Edström, Chem. Mater. 24 (2012) 1107.

[20] H. Hamze, M. Jimenez, D. Deresmes, A. Beaurain, N. Nuns, M. Traisnel, Appl. Surf. Sci. (2013).

[21] A.A. Galuska, J.C. Uht, N. Martinez, J. Vac. Sci. Technol. A 6 (1988) 110.

[22] M.P. Delplancke, J. Vac. Sci. Technol. A 9 (1991) 450.

[23] J. Światowska, V. Lair, C. Pereira-Nabais, G. Cote, P. Marcus, A. Chagnes, Appl. Surf. Sci. 257 (2011) 9110.

[24] M. Herstedt, D.P. Abraham, J.B. Kerr, K. Edström, Electrochim. Acta 49 (2004) 5097.

[25] C.K. Chan, R. Ruffo, S.S. Hong, Y. Cui, J. Power Sources 189 (2009) 1132.

[26] http://srdata.nist.gov/xps.

[27] G. Beamson, Surf. Sci. Spectra 3 (1994) 357.

[28] X. Liu, M.-C. Zheng, K. Xie, J. Power Sources 196 (2011) 10667.

[29] A. Avila, I. Montero, L. Galán, J.M. Ripalda, R. Levy, J. Appl. Phys. 89 (2001) 212.

[30] T. Asakawa, K. Tanaka, I. Toyoshima, Langmuir 4 (1988) 521.

[31] Z. Ma, T. Li, Y.L. Huang, J. Liu, Y. Zhou, D. Xue, RSC Adv. 3 (2013) 7398.

[32] W.X. Lei, Y. Pan, Y.C. Zhou, W. Zhou, M.L. Peng, Z.S. Ma, RSC Adv. 4 (2014) 3233.

## Figure captions

**Fig. 1.** SEM image of RAD material before milling.

**Fig. 2.** Raman spectrum of pyrolysed material, *inset*: The curve fit for the first order Raman spectra of studied material.

**Fig. 3.** The cv curves of RAD electrode in 1M $LiPF_6$ in EC/DMC in the potential range 0.005 – 3.2 V. The sweep rate v = 100 μV/s.

**Fig. 4.** The $20^{th}$ and $80^{th}$ charging/discharging curve of RAD, *inset:* the capacity vs. cycle number of RAD electrode material at different C – rates.

**Fig. 5.** Capacity vs. cycle number of RAD electrode for a fast charging/discharging process.

**Fig. 6.** XPS spectra of (a) C 1s (b) O 1s and (c) Si 2p core level of the RAD electrodes at different charge stages.

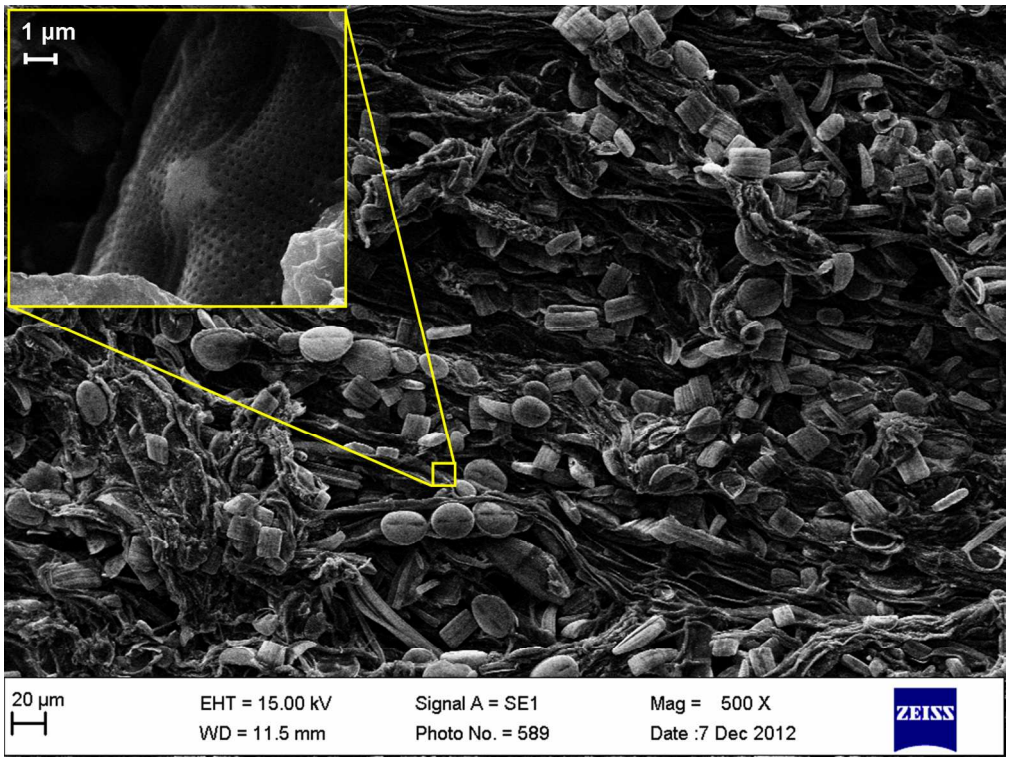


Fig. 1. SEM image of RAD material before milling.
135x101mm (300 x 300 DPI)

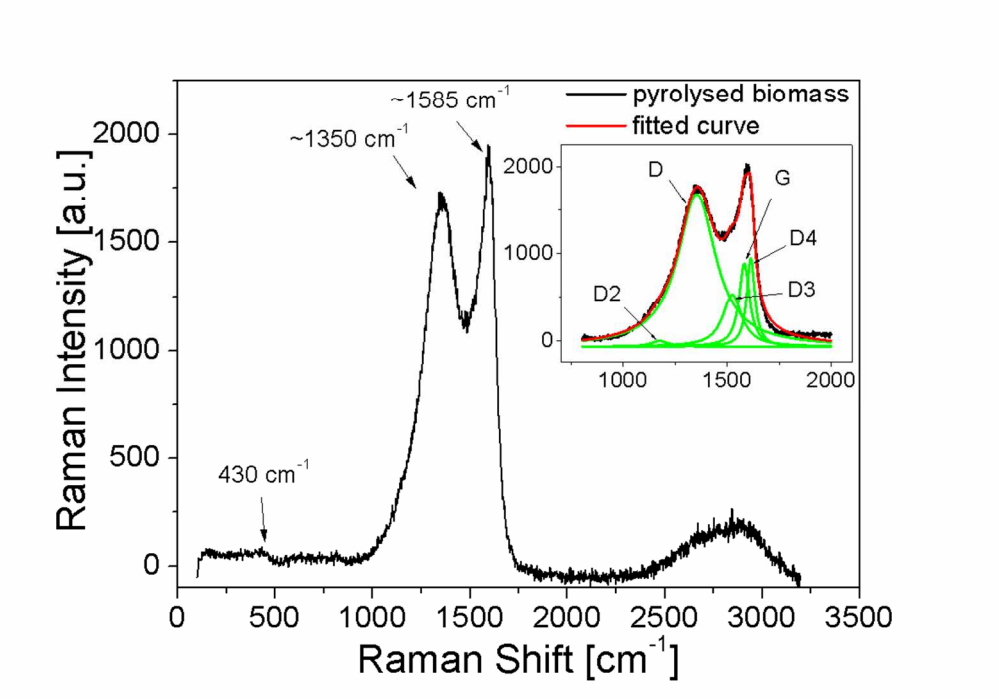


Fig. 2. Raman spectrum of pyrolysed material, inset: The curve fit for the first order Raman spectra of studied material.
99x70mm (300 x 300 DPI)

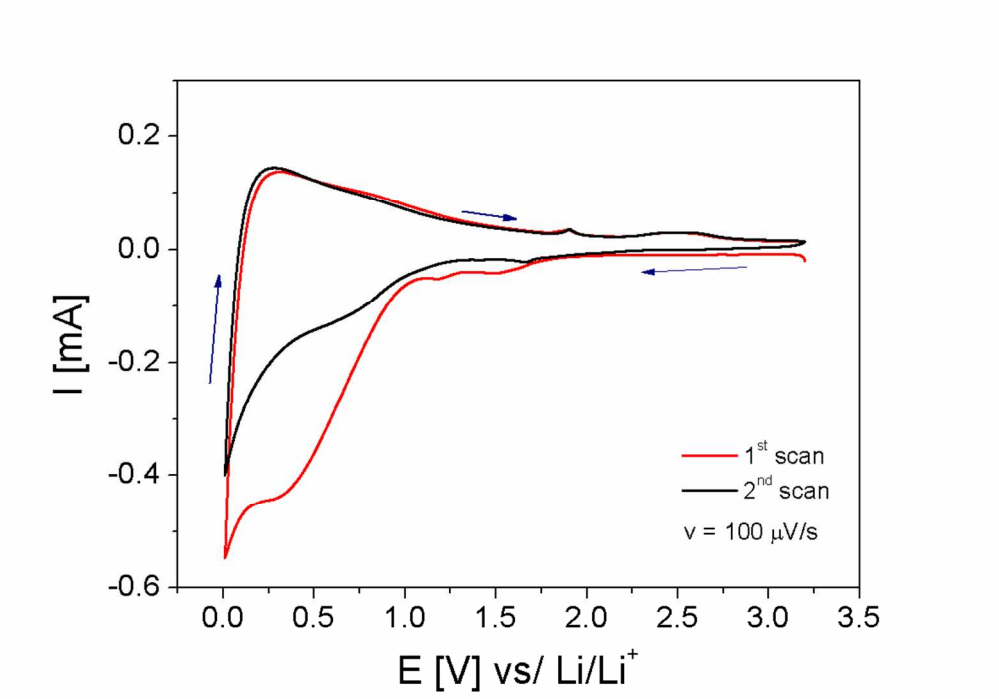


Fig. 3. The cv curves of RAD electrode in 1M LiPF6 in EC/DMC in the potential range 0.005 – 3.2 V. The sweep rate v = 100 μV/s.
99x70mm (300 x 300 DPI)

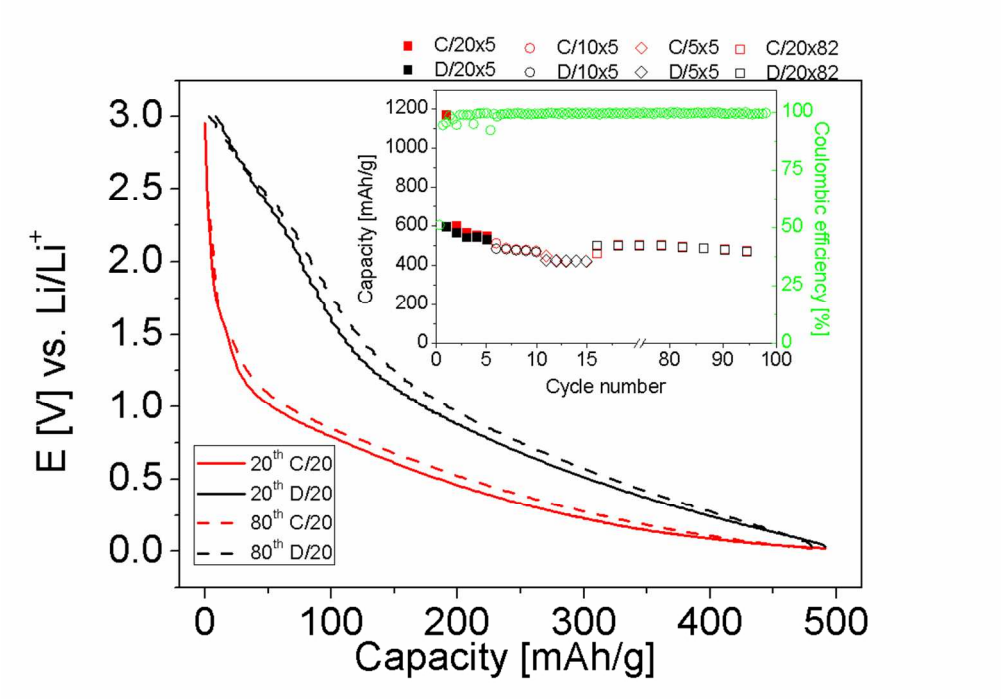


Fig. 4. The 20th and 80th charging/discharging curve of RAD, inset: the capacity vs. cycle number of RAD electrode material at different C – rates.
99x70mm (300 x 300 DPI)

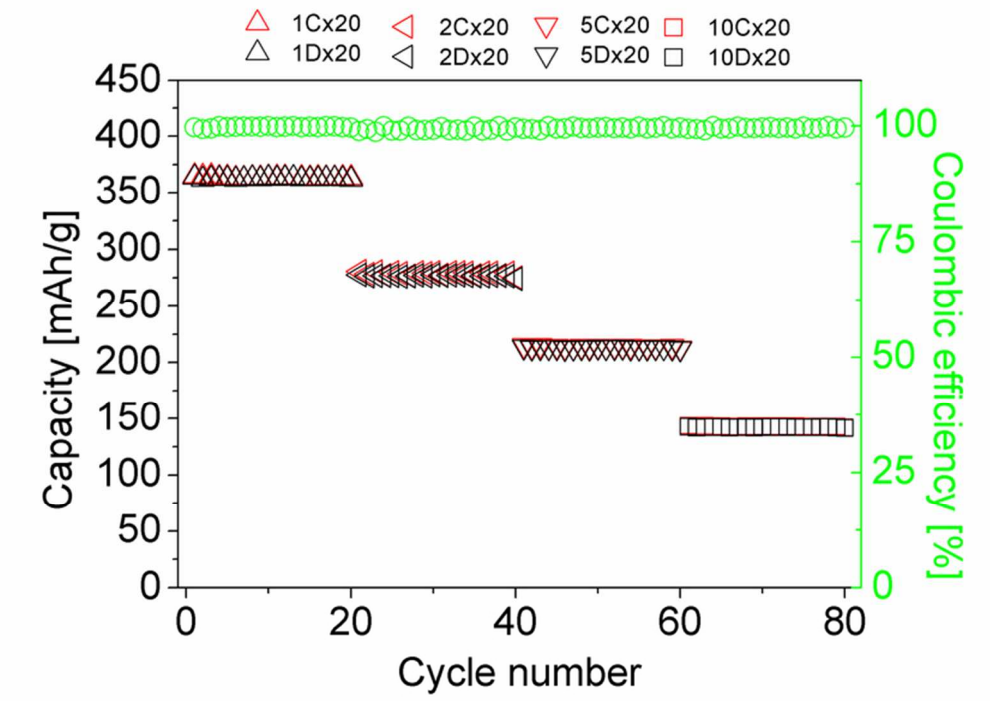


Fig. 5. Capacity vs. cycle number of RAD electrode for a fast charging/discharging process.
70x49mm (300 x 300 DPI)

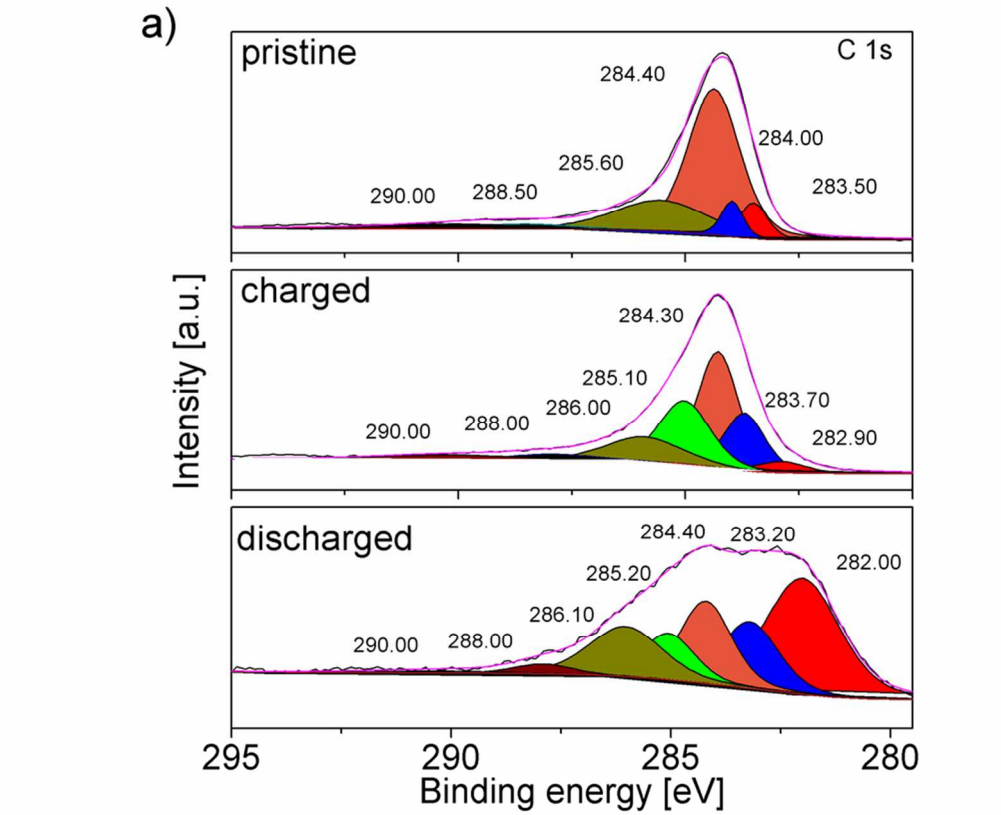


Fig. 6. XPS spectra of (a) C 1s (b) O 1s and (c) Si 2p core level of the RAD electrodes at different charge stages.
84x72mm (300 x 300 DPI)

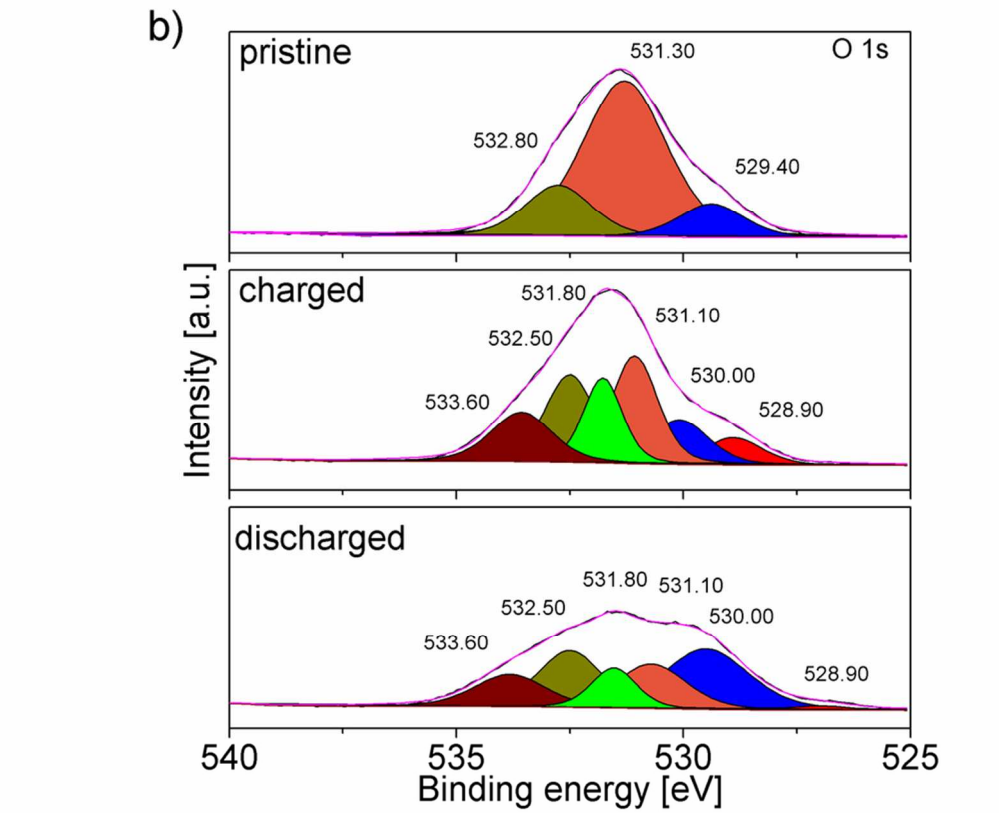


Fig. 6. XPS spectra of (a) C 1s (b) O 1s and (c) Si 2p core level of the RAD electrodes at different charge stages.
84x72mm (300 x 300 DPI)

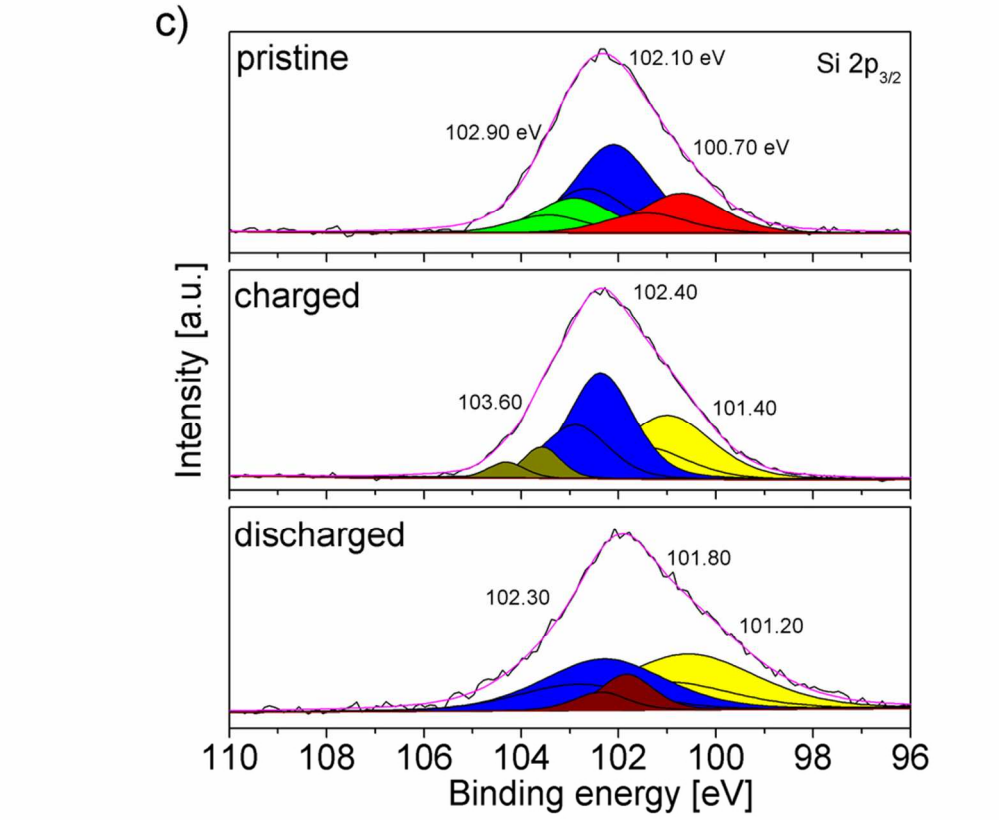


Fig. 6. XPS spectra of (a) C 1s (b) O 1s and (c) Si 2p core level of the RAD electrodes at different charge stages.
84x72mm (300 x 300 DPI)